Ballistic and Aerodynamic Characteristics Simulation for Trajectory Correction Projectile

Yongjie XU*, Fangdong DONG**, Nana ZHENG***

*College of Mechatronic Engineering, North University of China, 030051 Taiyuan, P.R. China,
E-mail: yongqiang515@nuc.edu.cn (Corresponding Author)
**No.208 Research Institute of China Ordnance Industries, 102202, Beijing, P.R. China, E-mail: dfd0415@126.com
***Changzhi Military Representative Office of Beijing Military Representative Bureau, 046000, Changzhi, P.R. China,
E-mail: 1357093356@qq.com

1. Introduction

With the continuous development of weapons and military equipment, fundamental changes in state-of-the-art war strategy have been observed, including the wide use of smart bombs, intelligent missiles, and precision-guided ammunition [1-4]. Current requirements for weaponry include both precision strikes on military installations and effective reduction of collateral damage to civilians and civilian infrastructure. Missiles have high hit accuracy, but their production and maintenance are very expensive, their number is limited, and their targets should have high value to substantiate their expenditure. A new kind of ammunition with relatively low cost, high precision, and damage efficiency is required to satisfy the modern war demands [5-7]. A probable solution is furnished by trajectory correction projectiles (TCPs). Noteworthy is that trajectory correction projectiles and missiles belong to two different precision attack categories, with the following fundamental differences. Missiles hit the targets directly by ballistic correction and require shooting with unfailing accuracy, while TCPs reduce the original shooting dispersion and improve the hit probability through several ballistic corrections. They have to hit a small-radius circular area with the target located in the center [8-10].

Using a 57 mm projectile as a design platform, trajectory correction projectiles with different aerodynamic layouts were designed. Combining the method of theoretical analysis with numerical simulation, the aerodynamic characteristic, static stability, exterior ballistic characteristic, and firing density of projectile were studied. Research results can provide technical support for the development of ballistic correction projectiles.

2. Modelling

2.1. Geometrical model

The projectile platform was based on SOCBT (secant ogive cylinder boat-tail) rotational stability projectile. To achieve the goal of trajectory correction, a drag-controlling device was installed in the projectile arc part. Specific parameters of the projectile platform were as follows: 230 mm in length, a diameter of 57 mm, a stern rake angle of 7, and geometry, is shown in Fig. 1.

The trajectory correction projectile took the form after installing the drag-controlling ring in the arc part as shown in Fig. 2. The distance between the installed drag-controlling ring and the top of projectile is 19.5 mm.
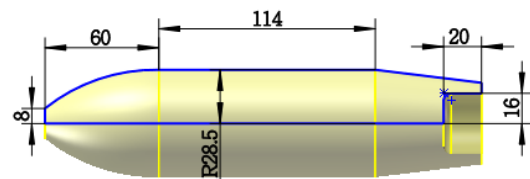

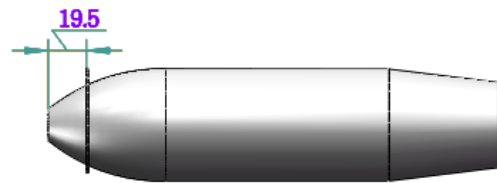Fig. 1 Schematic diagram of coordinate systems

Fig. 2 Diagram for TCP designing scheme

The original projectile was marked M 0, as shown in Fig. 3. According to different expansion heights after the drag-controlling ring's unfolding, three kinds of trajectory correction projectiles are designed, marked as M 1, M 2, and M 3, respectively. Their isometric views are depicted in Figs. 4 - 6, respectively.
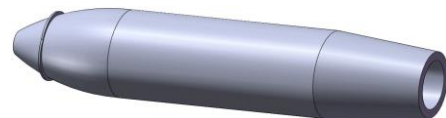

Fig. 3 Original projectile M 0

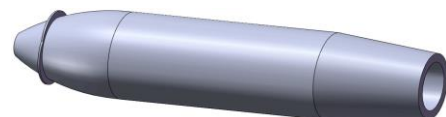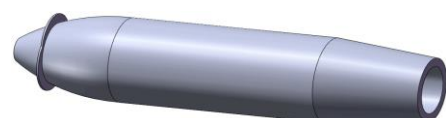Fig. 4 M 1 isometric view

Fig. 5 M 2 isometric view

Fig. 6 M 3 isometric view

Projectile mass properties, e.g., centroid position, were related to projectile flight stability. These properties of each projectile model are listed in Table 1.

The maximum radius with the unfolded drag-controlling ring was 27.1 mm, being less than the projectile radius of 28.5 mm. It was conducive to the flight stability of projectiles. This implied that the TCP design is reasonable.

Table 1

Mass properties of each projectile model

Code	Resistance ring expansion height /mm	Centroid position X, mm	Resistance ring unfold max radius, mm	Increased resistance area, mm²
M 0	——	16.3	——	——
M 1	3	16.2	23.1	310.0
M 2	5	16.2	25.1	535.4
M 3	7	16.2	27.1	767.3

2.2. Computational domain meshing

The pre-treatment used the Gambit software. The computational domain length and width were equal to the 20-fold projectile length and ten-fold projectile diameter, respectively. Due to the model's axial symmetry, the calculation domain covered only half of the model. The calculation domain diagram is depicted in Fig. 7, while the meshing quality report is summarized in Table 2.
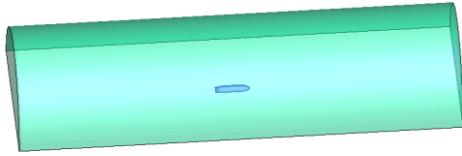

Fig. 7 Diagram for calculation domain

Table 2

Meshing quality report

From value	To value	Count in range	% of the total count
0	0.1	345276	9.61
0.1	0.2	355556	9.89
0.2	0.3	697721	19.41
0.3	0.4	1015026	28.24
0.4	0.5	562575	15.65
0.5	0.6	351262	9.77
0.6	0.7	205903	5.73
0.7	0.8	61228	1.70
0.8	0.9	0	0.00
0.9	1.0	0	0.00
0	1.0	3594547	100
Measured minimum value:3.90765e-007			
Measured maximum value:0.764016			

The maximum volume grid quality was 0.764, being less than the FLUENT fluid software quality ceiling grid of 0.97 [11]. Therefore, it can be used for numerical simulation.

The adopted computational procedure used a single-equation Spalart-Allmaras model [12-13] for turbulence, which has been widely used for solving the transport equation with the eddy viscosity, providing good results for the wall limit flow problem and inverse pressure gradient of the boundary layer problem. It is commonly applied to such aerodynamic problems of aircraft as streamlined flow around the airfoil profile, airflow field analysis, etc.

3. Analysis of aerodynamic characteristics

3.1. Aerodynamic numerical simulation

The numerical simulation utilized the following settings of the initial conditions according to references [14-15].

1. The grenade deflection angle and the angle of attack were 0°in the calculation, using density solver, Colin-Gaussian function gradient calculation method based on the nodes, and the single-equation Spalart-Allmaras turbulence model.

2. The WALL condition was a no-slip adiabatic viscous solid wall; the boundary condition was the far-field outer cylinder surface pressure.

3. Turbulence specification method used a turbulent viscosity ratio of 10.

4. The fluid physical properties were those of an ideal gas; viscosity was assessed via the Sutherland law, with an air density of 1.176674 kg/m³.

According to the fluid mechanics' theory, the dynamic viscous coefficient was expressed as follows:

$$\mu = \beta_a \cdot \frac{T^{1.5}}{T + T_s},\qquad(1)$$

where: μ is the dynamic viscous coefficient at the corresponding temperature; β_a=1.458×10⁻⁶ kg/(s·m·K^{1/2}) and Sutherland Constant T_s = 110.4 K. At an initial temperature T=15 °C or 288.15 K, we get the μ_{0N}=1.786×10⁻⁵ kg/(m·s·K^{1/2}).

5. Reference length and area of the calculation model were L = 0.057 m and S = 0.0026 m², respectively, at pressure P = 101325 Pa.

6. The aerodynamic convergence conditions determined the convergence, without setting the residual of each equation convergence criteria.

7. The flux types selected were the ROE-FDS Flux difference method for low Mach numbers and the AUSM method for high ones, which combination could accurately capture the shock wave and had good convergence.

8. Considering regional fluid's severe changes in the fluid mechanics' calculation, such as shock wave in the calculation of surface and its movement, the adaptive grid technology was used to improve the calculation precision.

Table 3

Calculation results on the drag coefficient

Mach	Drag coefficient			
	M 0	M 1	M 2	M 3
0.8	0.0904	0.1121	0.1670	0.2537
1.0	0.1357	0.1744	0.2322	0.3106
1.2	0.2037	0.2436	0.3035	0.3682
1.6	0.3091	0.4036	0.4703	0.5974
2.0	0.2730	0.3892	0.4507	0.5409
2.5	0.2746	0.3828	0.4516	0.5460
3.0	0.2689	0.3850	0.4688	0.5406

The Mach numbers were 0.8, 1.0, 1.2, 1.6, 2.0, 2.5,

and 3.0, involving the subsonic, transonic, and supersonic speed ranges. The drag-controlling ring heights were 3, 5, and 7mm. The calculation results on the drag coefficient are listed in Table 3.

The drag coefficient ratio was defined as the ratio between the drag coefficient values of the unfolded and folded drag-controlling rings. The respective results are summarized in Table 4.

Table 4

Drag coefficient ratios of each TCP

Mach	Drag coefficient ratios		
	M 1	M 2	M 3
0.8	1.2404	1.8471	2.8060
1.0	1.2853	1.7116	2.2892
1.2	1.1961	1.4898	1.8077
1.6	1.3056	1.5213	1.9325
2.0	1.4253	1.6507	1.9812
2.5	1.3938	1.6444	1.9881
3.0	1.4320	1.7435	2.0108

The classical aerodynamic simulation results were taken for comparison. Figs. 8 and depict the X-velocity and pressure nephograms, for the M 0 projectile with the Mach number of 2.5.
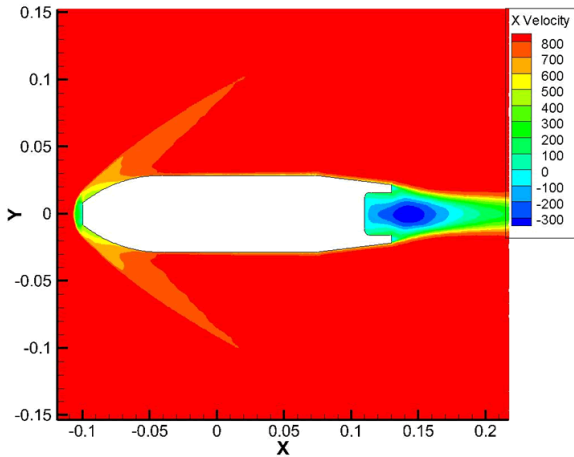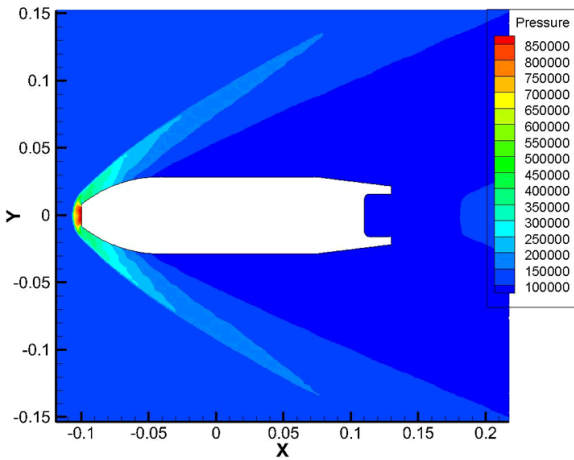

Fig. 8 X-velocity nephogram for M 0

Fig. 9 Pressure nephogram for M 0

Similarly, the X-velocity and pressure nephograms for the M3 projectile with the Mach number of 2.5 are plotted in Figs.10 and 11, respectively. Operation of the drag-controlling mechanism, operation changed the flow field

characteristics of the projectile in the position of this mechanism installation.
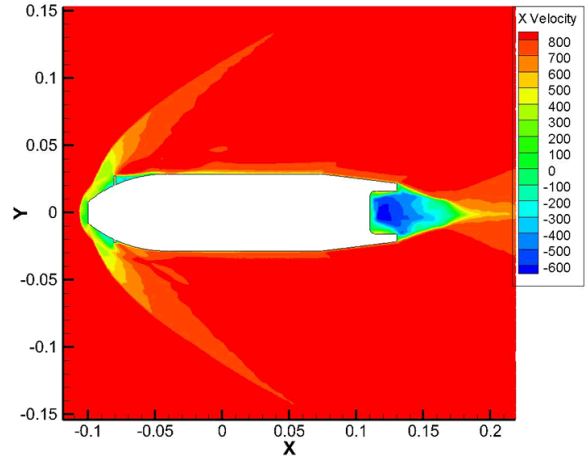

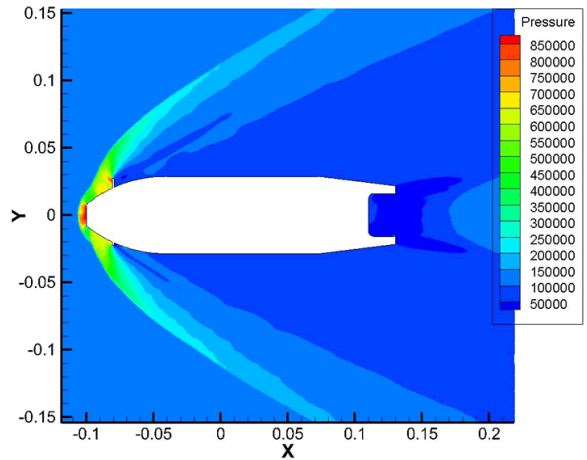Fig. 10 X-velocity nephogram for M 3

Fig. 11 Pressure nephogram for M 3

3.2. Static stability analysis

According to the theory of external ballistics [16], when the angle of attack exists, the flight attitude of the projectile is shown in Fig. 12.

Symbols p and c correspond to positions of pressure center and mass center, respectively. While h is the distance between pressure center and mass center, and l is the projectile length.

According to the theory of flight stability, the static stability reserve was defined as:

$$\frac{h}{l} \times 100\%. \tag{2}$$

The flying projectile should meet the requirement that the pressure center is behind the center of mass and the static stability reserve is greater than 10%, ensuring a stable flight.

Under the conditions of flight speed is 3Mach and attacking angle between -2° to +2°, a numerical simulation of the flying flow field of the projectile has been taken. The mean value of static stability reserve of each projectile model has been obtained, which is given as follow. Under the same conditions, the static stability reserve of the TCPs was increased by 2.03%, 4.37% and 7.30%, respectively, compared with the original projectile.
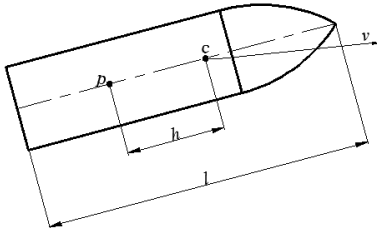
Fig. 12 Diagram of flying projectile

Table 5

Static stability reserve for each projectile

Code	M 0	M 1	M 2	M 3
Static stability reserve/%	11.39	13.42	15.76	18.69

Table 6

Standard atmospheric values at sea level

Temperature	Pressure	Air density	Virtual temperature	Speed of sound
t_{0N}=15℃	P_{0N}=100kPa	ρ=1.2603kg/m³	τ_{0N}=288.9K	c_s=341.1m/s

4. Calculation of external ballistics

To evaluate the correction ability of the correction mechanism, the particle trajectory calculation program was selected, which had a sufficient precision of shooting range and height recognition.

4.1. Trajectory model of the projectile of centroid

According to the external ballistics theory, variation of air temperature, air pressure, and air density with altitude follows certain rules. Under the artillery standard meteorological conditions, the provisions are given as follows.

The definitions of subscript are as follows: 0 is zero altitude; N is standard value; P is air pressure expressed as:

$$P = P_{0N} \cdot \pi(y). \tag{3}$$

ρ is air density expressed as:

$$\rho = \frac{\tau_{0N}}{\tau(y)} \cdot \pi(y) \cdot \rho_{0N}. \tag{4}$$

c_s is the speed of sound and expressed as:

$$c_s = \sqrt{k \cdot R_d \cdot \tau(y)}, \tag{5}$$

where: $\pi(y)$ is air pressure function; $\tau(y)$ is virtual temperature function; y is the height of projectile trajectory; k is air specific heat ratio and R_d is the gas constant. Furthermore, the expressions of air pressure function and virtual temperature function are given as follows:

$$\pi(y) = \begin{cases} (1 - 2.1904 \cdot 10^{-5} \cdot y)^{5.4} & (y \leq 9300) \\ 0.2923 \cdot exp\left\{-2.1206 \cdot \left[arctan\dfrac{2.3440 \cdot (y-9300) - 6328}{32221.0570} + 0.1939\right]\right\} & (9300 < y \leq 12000), \\ 0.1937254 \cdot exp\left[-\dfrac{y-12000}{6483.305}\right] & (12000 < y \leq 30000) \end{cases} \tag{6}$$

$$\tau(y) = \begin{cases} 288.9 - 0.006328 \cdot y & (y \leq 9300) \\ 230 - 6.328 \cdot 10^{-3} \cdot (y-9300) + 1.172 \times 10^{-6} \cdot (y-9300)^2 & (9300 < y \leq 12000). \\ 221.5 & (12000 < y \leq 30000) \end{cases} \tag{7}$$

To effectively simplify the problem and grasp the regularity and characteristics of flying projectile motion, establishing the projectile external ballistic model based on the following basic assumptions.

Assumption 1. Standard meteorological conditions, calm wind, and no rain.

Assumption 2. There is no mass eccentricity in the projectile; the centroid of the whole projectile is kept at the same point after the nose deflection, and the plane is exactly symmetric.

Assumption 3. Changes in the coriolis inertial force, gravity acceleration, and latitude changes are neglected.

Assumption 4. Changes in the earth's curvature and gravity acceleration and the changes in height are neglected; gravity acceleration is g = 9.80m/s², and it is applied in the vertical direction to the ground.

Assumption 5. No projectile spinning is assumed (i.e., the Magnus force, moment, damping moment, and angular moment in the empennage are neglected); the projectile is assumed to fly in the fore-and-aft plane.

The centroid motion kinematics equation, are given as follows:

$$\frac{dx}{dt} = V \cdot cos\theta, \tag{8}$$

$$\frac{dy}{dt} = V \cdot sin\theta, \tag{9}$$

where: x is a firing range; y is the height of projectile trajectory and θ is trajectory angle.

The missile body centroid dynamic equation, are given as follows:

$$m \cdot \left(\frac{dV}{dt}\right) = -R_X - m \cdot g \cdot sin\theta, \tag{10}$$

$$m \cdot V \cdot \left(\frac{d\theta}{dt}\right) = R_Y - m \cdot g \cdot cos\theta, \tag{11}$$

where: dV/dt is the tangential acceleration.

Based on the above four equations, Eqs. (12) - (15) can be derived:

$$\frac{dV}{dt} = \frac{-R_x - m \cdot g \cdot sin\theta}{m}, \tag{12}$$

$$\frac{d\theta}{dt} = \frac{R_y - m \cdot g \cdot cos\theta}{m \cdot V}, \tag{13}$$

$$\frac{dx}{dt} = V \cdot cos\theta, \tag{14}$$

$$\frac{dy}{dt} = V \cdot sin\theta. \tag{15}$$

The initial value setting: $t = 0$; $\theta = \theta_0$; $x = y = 0$ and $V = V_0$.

The four-stage Runge-Kutta method was applied in the simulations, due to its high accuracy and easy implementation in designing the program. A self-developed ballistic calculation program was written based on the above statement for the ballistic calculation of trajectory correction projectiles.

4.2. Ballistic calculation results

The basic parameters of ballistic calculations were as follows: a diameter of 0.05715 m, a weight of 0.66 kg, an initial velocity of 1050 m/s, a firing angle of 40°.

The ballistic calculation results of the original projectile model (M0), which contained no drag-controlling mechanism are summarized in Table 7.

Table 7

Exterior ballistic calculation results

Projectile posi-tion	Time /sec	Center of mass coordinate		Velocity m/s	Trajec-tory angle /°
		X/m	Y/m		
muzzle data	0.00	0.00	0.00	1050.00	40.00
vertical data	18.09	4331.61	2465.05	151.99	0.00
placement data	43.18	7126.41	0.00	184.02	-66.52

The external ballistic characteristics of the original M 0 projectile and the trajectory correction projectiles M 1, M 2, and M 3 can be reflected by the relationship between the shooting range and the shooting height, as shown in Fig. 13.
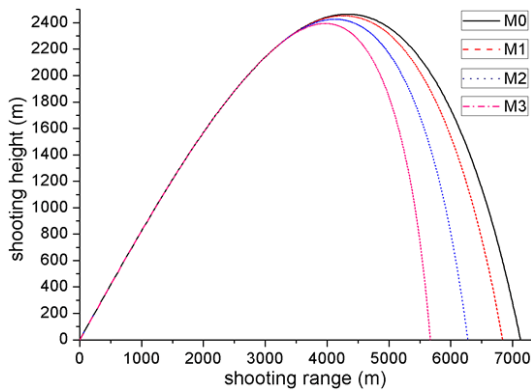

Fig. 13 Relationship of firing range and height

4.3. Correction ability calculation

The correction ability was defined as $\Delta X = X_0 - X_C$, where ΔX is the correction shooting range; X_0 is the firing range without the drag-controlling device and X_C is the firing range with the operating drag-controlling device. The particular results of the calculated range corrections are listed in Table 8.

Table 8

Correction value of shooting ranges

The resistance ring unfold time /sec	Correction values of shooting ranges /m		
	M 1	M 2	M3
10	287.24	852.08	1457.69
12	231.75	702.54	1228.74
14	186.74	577.70	1032.21
16	150.06	473.13	863.02
18	119.98	385.13	716.82
20	95.15	310.67	589.84
22	74.53	247.32	478.95
24	57.31	193.19	381.70
26	42.95	147.01	296.45
28	31.07	107.91	222.17
30	21.41	75.40	158.50
32	13.80	49.19	105.51
34	8.08	29.09	63.54
36	4.09	14.83	32.84
38	1.62	5.90	13.15
40	0.40	1.44	3.18
42	0.02	0.08	0.17

4.4. Firing density calculation

To analyse the ground density of the projectile, the Monte Carlo method [17] is used to simulate projectile firing under certain initial conditions that listed in Table 9.

The expressions of distance and direction middle deviation are as follows:

$$E_x = 0.6745\sqrt{\frac{\sum_{i=1}^{n}(x_i - x_{cp})^2}{n-1}}, \tag{16}$$

$$E_z = 0.6745\sqrt{\frac{\sum_{i=1}^{n}(z_i - z_{cp})^2}{n-1}}, \tag{17}$$

where: E_x and E_z are the distance and direction intermediate deviations, respectively, while x_i and z_i are the impact point coordinates.

The expressions of the average impact point coordinates x_{cp} and z_{cp} are as follows:

$$x_{cp} = \sum_{i=1}^{n} x_i \bigg/ n, \tag{18}$$

$$z_{cp} = \sum_{i=1}^{n} z_i \bigg/ n, \tag{19}$$

where: n is the number of projectiles in one group (equal to 5000 in the simulation).

The statistical results on distance and direction intermediate deviations of the projectile dispersion are listed in Table 10.

Table 9
Initial conditions for simulation

Parameter	Mean value	Standard deviation
Velocity/m/s	1050	52.50
Weight/kg	0.66	0.03
Trajectory angle/°	40	2.00

Table 10
Results of the firing density simulation

Code	x_{cp}	z_{cp}	E_x	E_z	Firing density
M0	7136.299	7.102	99.511	0.15	0.0139
M1	5969.994	5.422	81.721	0.112	0.0114
M2	4741.056	3.813	69.369	0.083	0.0124
M3	3641.239	2.548	56.858	0.059	0.0133

The results show that the firing densities of M 1, M 2 and M 3 exceeded that of M0 by 18.01%, 10.91% and 3.91%.

5. Conclusions

This study used numerical simulations and engineering calculations to assess the aerodynamic characteristic, static stability, exterior ballistic characteristic and firing density of several trajectory correction projectile(TCPs). And the following conclusions could be drawn:

1. TCPs with different aerodynamic configurations were designed based on the 57mm diameter rotation stability projectile. The numerical simulation of the flight flow field for different projectiles was performed via the FLUENT software, yielding the aerodynamic parameters for different Mach numbers.

2. According to the external ballistics theory, the static stability reserves of each projectile were calculated, showing that the static stability of TCPs was improved by 2.03%-7.30% compared with the original projectile.

3. According to the artillery standard meteorological conditions, the projectile centroid kinematics dynamics and motion equations of the projectile's mass center under the ground rectangular coordinate system were derived. The numerical simulation results of projectile external ballistic motion indicated that the correction value of shooting range of the TCPs under study reached 1457.69 m.

4. The calculation of the firing density of each TCP under study was executed via the Monte Carlo method under the test conditions with 5000 repeated times. Its results indicated that the firing density of TCPs with the proposed improvement increased by 3.91 %-18.01 %.

Conflict of interests

The authors declare that there is no conflict of interests regarding the publication of this paper.

Acknowledgments

References

1. **Xia, B.; Zhou L.** 2013. Trajectory correction projectile and analysis on the key technologies for the trajectory correction process, National Defence Science & Technology 34(3):27-33 (in Chinese). http://dx.doi.org/10.3969/j.issn.1671-4547.2013.03.006.
2. **Deng, Z. L.; Shen, Q.; Cheng, J. S.; Wang, H. Y.** 2020. Trajectory estimation method of spinning projectile without velocity input, Measurement160: 1-8. http://dx.doi.org/10.1016/j.measurement.2020.107831.
3. **Sun, X. T.; Gao, M.; Zhou, X. D.; Lv, J.** 2021. Guidance simulation and experimental verification of trajectory correction mortar projectile, IEEE Access 9: 15609-15622. http://dx.doi.org/10.1109/ACCESS.2021.3052883.
4. **Zhang, T.; Zhao, X. L.** 2014. Analysis of trajectory correction projectile and its key technology, Aerodynamic Missile Journal 5: 38-42 (in Chinese). http://dx.doi.org/10.16338/j.issn.1009-1319.2014.05.015.
5. **Shen, Q.; Zhou P.; Yang D. H.; Li, D. G.** 2013. Correction strategy analysis on one-dimensional trajectory correction fuze, Transactions of Beijing Institute of Technology 33(5): 445-448 (in Chinese). http://dx.doi.org/10.3969/j.issn.1001-0645.2013.05.006.
6. **Zhang, Y. W.; Gao, M.; Yang, S. C.; Fang, D.** 2015. Optimization of trajectory correction scheme for guided mortar projectiles, International Journal of Aerospace Engineering 2015: 1-14. http://dx.doi.org/10.1155/2015/618458.
7. **Yin, J. P.; Wang, Z. J.** 2014. Ammunition Theory, Beijing Institute of Technology Press. 590 p. (in Chinese).
8. **Yang, F.; Hao, Y. P.; Bu, G. L.** 2011. Design and study for area-changing and damp-increasing range correction system, Journal of Projectiles Rockets Missiles and Guidance 31(3): 165-169 (in Chinese). http://dx.doi.org/10.3969/j.issn.1673-9728.2011.03.048.
9. **Zhao, H.; Su, Z.** 2020. Real-time estimation of roll angle for trajectory correction projectile using radial magnetometers, IET radar, sonar & navigation 14(10): 1559-1570. http://dx.doi.org/10.1049/iet-rsn.2020.0136.
10. **Arnoult, G.; Zeidler,M.; Garnier, E.** 2020. Control surface geometry surrogate-based optimization for spin-stabilized projectile course correction, AIAA journal 58(2): 550-560. http://dx.doi.org/10.2514/1. J058323.
11. **YU, Y.** 2011. Fluent Introductory and Advanced Tutorial. Beijing Institute of Technology Press. 292p. (in Chinese).
12. **Rollet-Miet, P.; Ferziger, J.; Laurence, D.** 999. LES and RANS of turbulent flow in tube bundles, International Journal of Heat and Fluid Flow 20(3): 241-254. http://dx.doi.org/10.1016/S0142-727X (99)00006-5.
13. **Wissink, J. G.** 2003. DNS of separating low Reynolds number flow in a turbine cascade with incoming wakes, International Journal of Heat and Fluid Flow 24(4): 626-635. http://dx.doi.org/10.1016/S0142-727X (03)00056-0.
14. **Lei, X. Y.; Zhang, Z. A.; Du, Z. H.** 2019. Analysis of an improved trajectory correction scheme based on mass

blocks, Journal of Systems Engineering and Electronics 30(1): 180-190.

http://dx.doi.org/10.21629/JSEE.2019.01.17.

15. **Ning, X. L.; Wu, Y. X.; Yu, T. P.; Chen, W. B.** 2016. Research on comprehensive validation of simulation models based on improved grey relational analysis, Acta Armamentarii 37(2): 338-374 (in Chinese).

http://dx.doi.org/10.3969/j.issn.1000-1093.2016.02.021.

16. **Han, Z. P.** 2014. Exterior Ballistics of Projectiles and Rockets. Beijing Institute of Technology Press, 617p. (in Chinese).

17. **Chen, K.; Huang, H. Y.; Han, W. J.; Feng, G. T.** 2010. numerical research of air cooling turbine using one way aerodynamic and thermal mechanical conjugate method, Science Technology and Engineering 10(3): 726-732 (in Chinese).

http://dx.doi.org/10.3969/j.issn.1671-1815.2010.03.029.

Y. Xu, F. Dong, N. Zheng

BALLISTIC AND AERODYNAMIC CHARACTERISTICS SIMULATION FOR TRAJECTORY CORRECTION PROJECTILE

S u m m a r y

Conventional ammunition easily deviates from the intended target. Its hit probability is reduced by such disturbance factors as fabrication errors, initial muzzle disturbance, initial velocity probable error, and stochastic wind effect. The effect of the above interference factors can be reduced by improving the shooting dispersion, ammunition, and gun or rocket engine structure. However, such improvements may fail to meet the operational requirements for modern warfare. Ballistic correction technique is a proposed trajectory control technique for precision strike with effective damage. Taking a 57 mm calibre projectile as research object, trajectory correction projectile with different aerodynamic layouts were designed. The aerodynamic characteristic, static stability, exterior ballistic characteristic and firing density of each projectile has been studied through research method of theoretical analysis and numerical calculation. These findings are considered instrumental in the trajectory correction technology research and engineering application.

Keywords: trajectory correction projectile, ballistic characteristic, trajectory model, numerical simulation.